UNIVERSITAT DE BARCELONA

Spin crossover supramolecular coordination compounds: design, synthesis and properties

Mohanad D .Darawsheh

Contents

CHAPTER 6: Magneto-Structural Correlations

6.1 Introduction

The distortion of the Fe(II) cation in the high spin (HS) state has been previously studied for poly-pyrazolylpyridine systems[1–4] and for systems with $[Fe(II)L_n(NCS)_2]$ formula[5] where L_n are chelating nitrogen based ligands. The distortion parameters Σ and Θ have been used to evaluate the degree of distortion of the Fe(II) coordination from the ideal octahedron. These two parameters are defined in chapter 1 and have been used to analyze and describe the SCO compounds in the previous chapters. Σ measures the local angular distortions of the octahedral donor set as defined with the equation $\sum_{i=1}^{12} |90 - a_i|$, where a_i are the are the 12 cis-N-Fe-N angles at the Fe(II) centre.[1,2] Θ measures the degree of the trigonal distortion of the coordination geometry from octahedral toward a trigonal prism using the equation $\sum_{i=1}^{24} |60 - \theta_i|$, where θ_i are the 24 unique N-Fe-N angles measured on the projection of two triangular faces of the octahedron along their pseudo-threefold axis.[1,2] Continuous symmetry measures are another excellent tool to study the relationship between the geometry of a metal center and the spin transition. Two possible ideal symmetries are considered, the ideal octahedral [*S(Oh)* = 0] and the ideal trigonal prism [*S(itp)* = 0] with the pathway between both following the Bailar twist maintaining the *D3* symmetry at all times (see chapter 1).[6] These studies clearly shown that the HS species is always more distorted than the LS counterpart from the ideal octahedral geometry. It has also been shown that the extreme distortion of the HS state very often trap the system in the HS state.[7] In this chapter, the influence of the distortion around Fe(II) on the occurrence of SCO will be studied. The second part of this chapter includes Hirshfeld surface analyses,[8] which describe the supramolecular intermolecular interactions and the crystal packing in the various compounds of this thesis. Such analyses are increasingly becoming common place in SCO research.[4,9–11]

6.2 Coordination Geometry of Fe(II) Vs. Occurrence of SCO

A compilation of the distortion parameters and the continuous symmetry measures for all the compounds obtained in this thesis and related compounds found in the literature, with three bidentate pyrazolylpyridine moieties around the Fe(II) center, are given in

Table 6.1 and 6.2. Σ values fall in the range 57.00 to 69.76˚ for the LS Fe(II) centers whereas the HS state Fe(II) centers exhibit values above 87.9˚. The Fe(II) centers trapped in the HS state exhibit Σ values above 106.94˚. Θ values fall below 220˚ and above 265˚ for LS and HS centers, respectively. Again the Fe(II) centers that trapped in the HS state exhibit higher distortions with values higher than 310˚.

Table 6.1: Distortion measurements for all the dinuclear Fe (II) compounds presented in this thesis.

Compound	Fe assignment	Spin state (Temp/K)	Σ/˚	Θ/˚	*S(Oh)*	*S(itp)*	$(Fe\text{-}N)_{avg}$/Å
v	Fe1	LS (100)	60.6	194.0	0.708	14.529	1.960
	Fe2	LS (100)	66.8	207.0	0.760	14.948	1.975
1	Fe1	HS (100)	115.77	337.4	3.523	7.256	2.189
		HS (310)	111.08	322.9	3.234	7.609	2.191
		HS (340)	111.07/	316.0	3.102	7.940	2.190
	Fe2	LS (100)	58.79	176.3	0.755	12.815	1.979
		Mixed (310)	76.82	231.1	1.377	10.985	2.066
		HS (340)	90.75	274.0	1.989	9.728	2.137
2	Fe1	HS (100)	113.63	325.8	3.274	7.402	2.193
		HS (280)	109.76	313.8	3.020	7.978	2.189
		HS (340)	106.94	306.3	2.843	8.377	2.186
	Fe2	LS (100)	61.22	186.9	0.809	12.862	1.980
		Mixed (310)	84.30	256.1	1.616	10.872	2.099
		HS (340)	95.51	286.2	2.148	9.590	2.173
1a	Fe1	LS (90)	62.5	188.0	0.942	11.909	1.984
		Mixed (215)	75.1	244.1	1.458	10.666	2.047
		HS (300)	95.4	282.9	2.425	9.036	2.156
2a	Fe1	LS (90)	64.19	194.7	1.006	11.741	2.000
		Mixed (195)	86.88	257.2	1.932	9.871	2.115
		HS (296)	96.92	288.1	2.467	9.013	2.176
3	Fe1	HS (100)	106.6	331.7	3.383	6.344	2.185
	Fe2	HS (100)	110.78	335.7	3.610	5.896	2.189
4	Fe1	HS (100)	107.56	330.5	3.322	6.497	2.191
	Fe2	HS (100)	109.04	326.7	3.303	6.450	2.192
5	Fe1	LS (100)	61.77	199.1	0.731	15.418	1.950
6	Fe1	LS (100)	59.61	181.2	0.753	13.771	1.986
	Fe2	LS (100)	59.81	185.2	0.737	14.355	1.980
7	Fe1	LS (100)	63.84	201.3	0.726	15.476	1.969
8	Fe 1	LS (100)	65.08	200.2	0.763	14.920	1.968
	Fe2	LS (100)	58.01	184.1	0.706	14.492	1.971
9	Fe1	LS (100)	57.96	183.2	0.684	14.863	1.972
10	Fe1	LS (100)	69.76	213.3	0.774	15.053	1.961
	Fe2	LS (100)	64.69	202.0	0.732	14.722	1.959
11	Fe1	LS (100)	59.8	184.2	0.645	14.534	1.954
		LS (250)	62.0	191.3	0.692	14.358	1.960
		LS (280)	57.0	184.1	0.676	14.308	1.960
	Fe2	LS (100)	61.7	198.4	0.769	14.021	1.980
		Mixed (250)	76.8	241.2	1.231	12.585	2.090
		HS (280)	88.0	274.2	1.654	11.693	2.135

Table 6.2: Distortion measurements for compounds containing Fe (II) surrounded by three bidentate pyrazolylpyridine moiety found in the CSD.

Reference Code	Spin state (Temp/K)	Σ/°	Θ/°	*S(Oh)*	*S(itp)*	$(Fe\text{-}N)_{avg}$/Å
DUMBUJ[12]	HS (293)	96.1	301	2.353	10.943	2.157
KAJXUQ[13]	LS (100)	69.5	204.6	0.878	14.166	1.988
KINQUT[14]	LS (100)	61.0	190	0.737	15.008	1.967
LENXUY[15]	LS (100)	57.4	182	0.682	14.801	1.984
NIHWIM[16]	HS (100)	127.1	329.2	2.977	9.567	2.207
NIHYEK[16] **(Fe6)**	HS (100)	90.7	284	1.827	12.182	2.194
NIHYEK[16] **(Fe7)**	HS (100)	87.9	270	1.655	12.716	2.159
PUHXOG[17]	HS (293)	85	252	1.662	11.596	2.114
REXBON[18]	LS (100)	64	189	0.764	14.454	1.983
REXBUT[18]	HS (300)	90.0	270	1.968	10.798	2.133
REXCAA[18]	LS (100)	61.4	185.2	0.860	13.072	1.987

Only 10 compounds were found in the CSD data where three pyrazolepyridine ligands surround Fe(II) centers. The only three that exhibit SCO are compounds KINQUT[14], REXBON (the same compound as REXBUT which is the HS crystal structure)[18] and REXCAA[18] (Table 6.2). Plots of Σ vs. Θ for all available data are presented in Figure 6.1. The compounds have been divided into these in the LS state without SCO at high temperatures, LS state centers that exhibit SCO (the data available only for the LS state), Fe(II) centers trapped in the HS state, Fe(II) centers with data available at variable temperatures and for selected compounds from the literature. The correlation between Σ and Θ follows a trend seen before in polypyrazolylpyridine ligands.[2,3] The most interesting observation is the higher distortion exhibited by the Fe(II) centers that do not exhibit SCO. It was shown that the high distortion of the Fe(II) centers traps these centers in the HS state even at low temperatures, which explained as kinetic effect depending on theoretical calculations.[19] The HS Fe(II) centers that exhibit SCO show less distortion and fall closer to the region of the mixed spin centers (Figure 6.1).

There are no magnetic studies for compounds DUMBUJ[12] and PUHXOG[17]. However, the distortion exhibited by these compounds in the HS state at 293 K suggests the occurrence of SCO at low temperatures since these values correspond to these of mixed spin centers. In the case of NIHYEK[16] (Fe6) NIHYEK[16] (Fe7), the Fe(II) centers are located in a helical structure close to an Fe(III) and Fe(II) centers with which they are antiferromagnetically coupled. The ligand in this compound is very similar to H_2L4 in

this thesis and the distortion around the metal ions falls in the range of Fe(II) centers that exhibit SCO. It possible that the antiferromagnetic interaction prevents the observation of SCO in this compound.

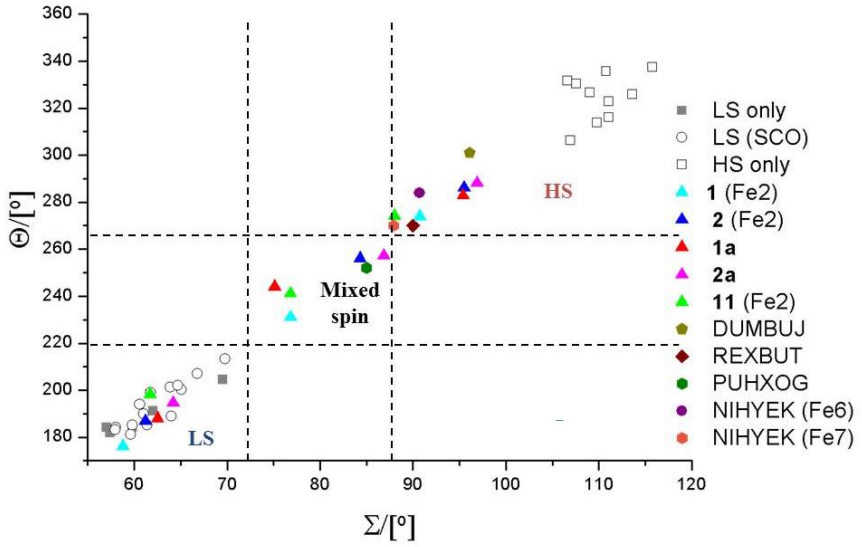

Figure 6.1: Representation of Θ and Σ for structural data available from this thesis and the CSD for compounds with Fe(II) center surrounded by three bidentate pyrazolyl-pyridine ligands.

Most of the compounds in the LS state at 100 K exhibit SCO at higher temperatures although in some cases it is not yet complete at 400 K, as in compounds **5**-**10**. This indicates the suitability of the crystal field environment of pyrazolylpyridine for SCO. The Θ vs. Fe-N_{avg} plot (Figure 6.2) correlates well with the spin transition of the compounds, similar to what is seen in the previous plots. Again the separation between the HS and the LS states is obvious.

The plot of continuous symmetry measures *S (Oh) vs S (itp)* is shown in Figure 6.3. The LS Fe (II) centers exhibit a smaller *S(Oh)* values and higher *S(itp)* values indicating more regular octahedral symmetry. When going to the HS state, the distortion towards the trigonal prism is obvious. The Fe(II) centers trapped in the HS state exhibit high *S(Oh)* values and smaller *S(itp)* values than these for HS Fe(II) centers that exhibit SCO. The distribution of the data deviate slightly from the ideal Bailar twist which is attributed to the geometry constraints of the chelating ligand.[6,20] The dependence of the octahedral symmetry measure on the Fe-N_{avg} is similar to the one seen in the Θ vs. Fe-

N_{avg} plot, where again there is a clear separation between the HS and LS state complexes.

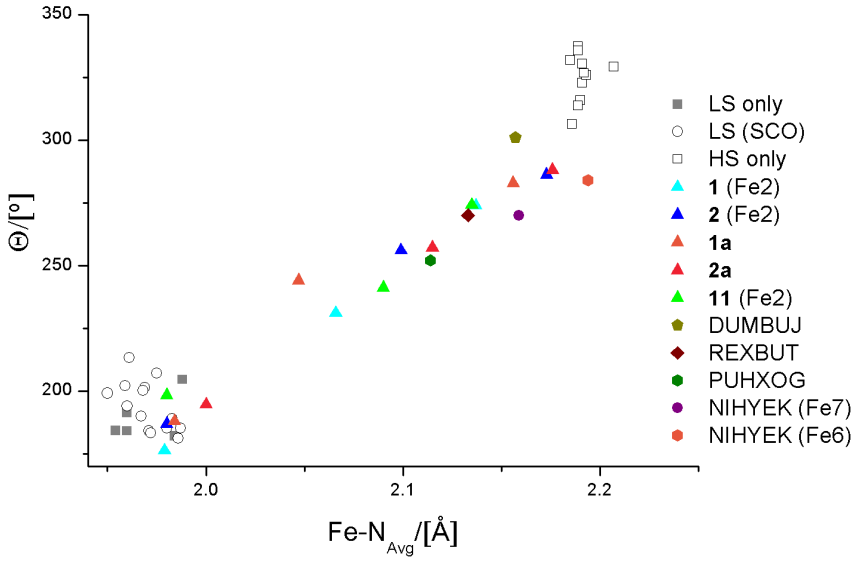

Figure 6.2: Representation of Θ vs. Fe-N_{avg} for structural data available from this thesis and the CSD for compounds with Fe(II) center surrounded by three bidentate pyrazolyl-pyridine ligands.

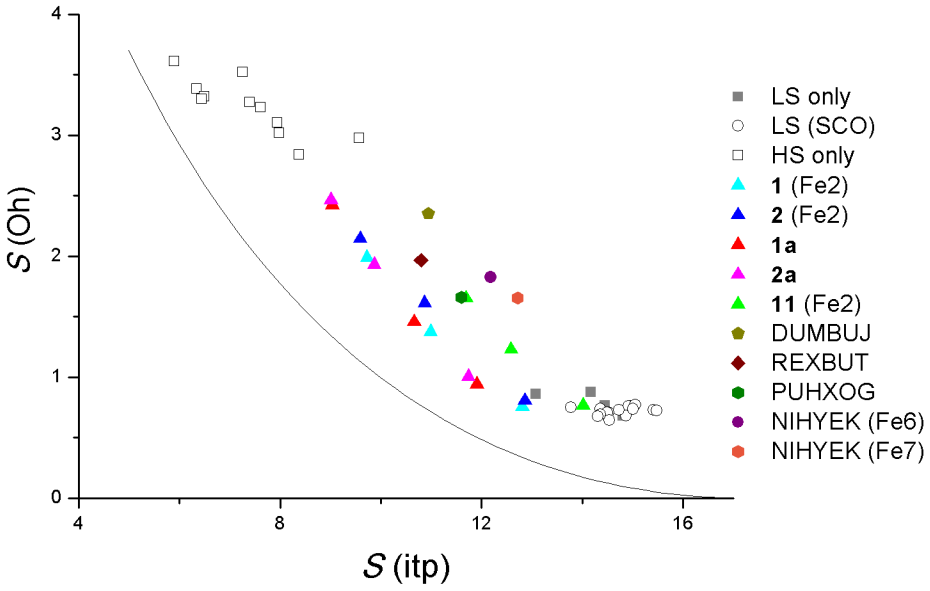

Figure 6.3: Plot of the octahedral *S(Oh)* and trigonal prismatic *S(itp)* symmetry measures for all of the Fe (II) compounds with three bidentate pyrazolylpyridine ligands. The solid line represents the ideal Bailar twist pathway.[20]

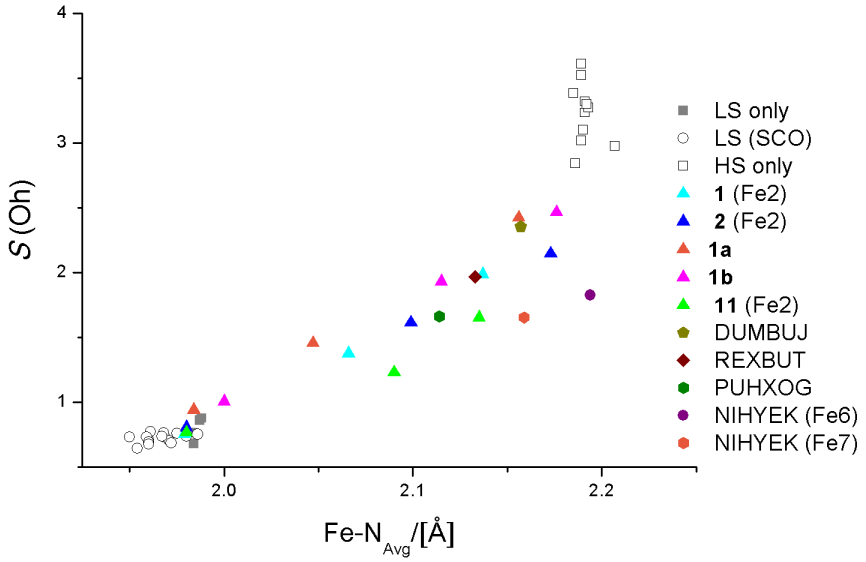

Figure 6.4: Representation of S(Oh) vs. Fe-N_{avg} for structural data available from this thesis and the CSD for compounds with Fe(II) center surrounded by three bidentate pyrazolyl-pyridine ligands.

6.3 **Hirshfeld Surface Analysis**

The compounds synthesized in this thesis feature a lot of supramolecular interactions involving the host and the guest entities in addition to anions and solvent molecules. These intermolecular interactions arise for the most part from the functional groups (N-H, benzyl and pyridyl groups) found in the ligands. The program crystalExplorer 3.1[21] allows the calculation of Hirshfeld surfaces in the crystal lattice, which give information about the crystal packing and the strength of the intermolecular interactions within the lattice. A Hirshfeld surface is a surface that separates any volume of the crystal from the rest of the space, where the electron density of the enclosed "molecule" (the promolecule) equals the contribution by its neighbors (procrystal).[8] In this way, the crystal can be partitioned into non-overlapping regions, which allows for mapping a wide range of functions on these surfaces and thus visualizing several properties that vary across the molecule of interest. For example, the property d_{norm} may be mapped in the Hirshfeld surface and gives a visual description of the strength of the contacts across the whole molecule via a color scale. The strongest interactions which have short contacts has an extreme red color and for weakest interactions with long contacts have

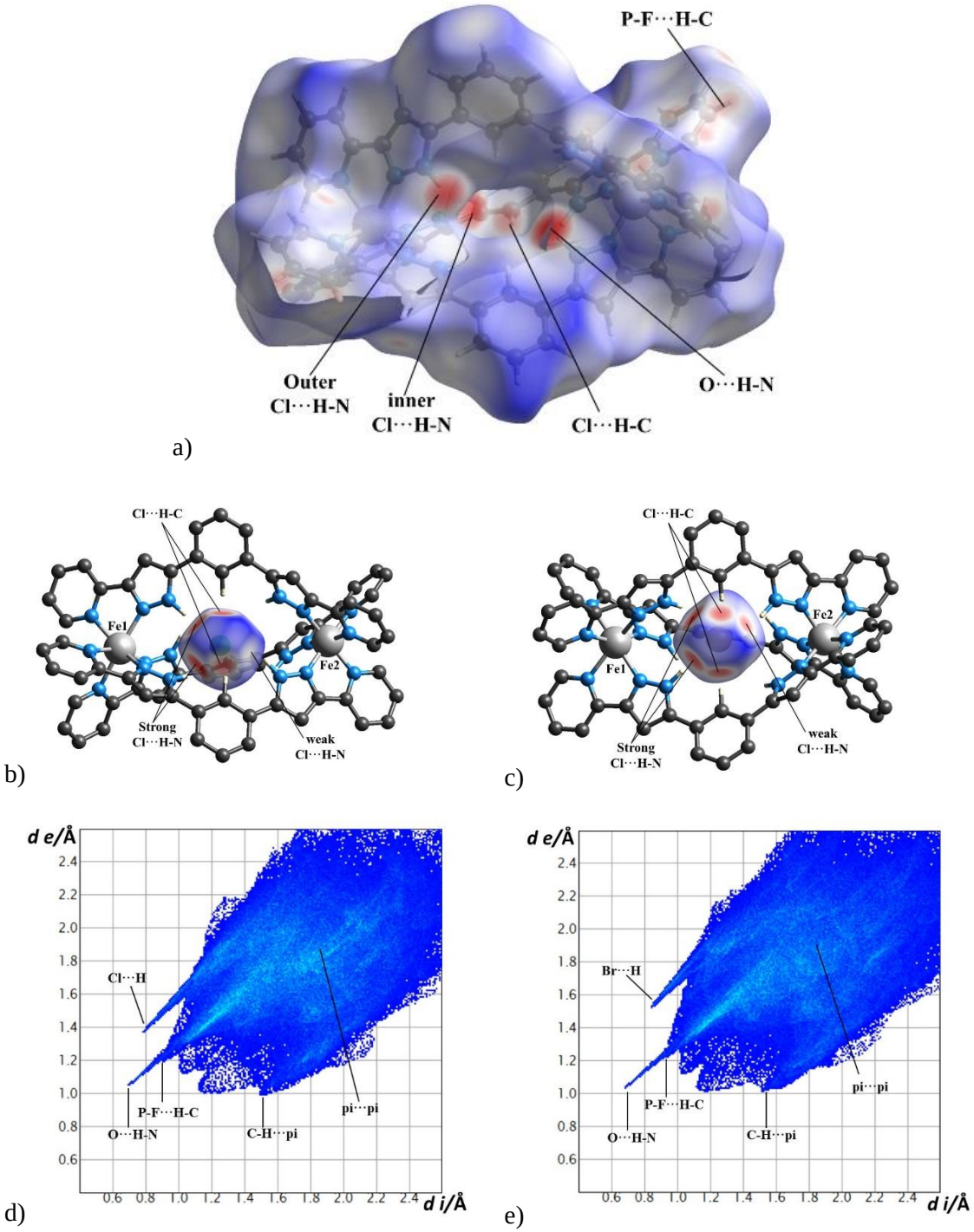

Figure 6.5: Hirshfeld surface of the a) $[Fe_2(H_2L4)_3]^{4+}$ cation from compound **1**, b) chloride guest in compound **1**, c) bromide guest in compound **2**, and the 2*D* fingerprint derived from the helicase's Hirshfeld surfaces of compound **1** (d) and compound **2** (e).

the blue color passing through white for intermediate interactions. All the points in the Hirshfeld surface can be represented in the form of 2*D* fingerprint plots.[22] This Fingerprint plots provide a correlation between d_e and d_i, which correspond to the

distance to the nearest external and internal atoms, respectively. The color of the 2*D* graph indicates also the density of the points in the region. The red color indicates high number of interactions corresponding to that [d_e,d_i] region and with decreasing the density of the points the color goes to blue passing through green. The fingerprint plots give information about the type, the density and the strength of the interactions.

These types of studies can be useful in SCO compounds where the change in the SCO behavior can be understood on the basis of the intermolecular interactions. It could be applied in the compounds in this thesis since the same cationic helicate exhibits different SCO behavior by small alteration in the supramolecular interactions of anions or solvent molecules.

The Hirshfeld surface for the $[Fe_2(H_2L4)_3]^{4+}$ helicate and the chloride guest in compound **1**, bromide guest in compound **2**, and the fingerprint plots of the $[Fe_2(H_2L4)_3]^{4+}$ helicate in compounds **1** and **2** are seen in Figure 6.5. One can see from the Hirshfeld surface of $[Fe_2(H_2L4)_3]^{4+}$ helicate in compound **1** that the most important interactions are Cl···H-N, O···H-N and Cl···C-H. The interaction of the N-H groups with methanol molecules is stronger than that with chloride which is indicated by the darker red color. This result can be seen at the fingerprint plot, where the O···H-N area reaches shorter (d_e, d_i) values of around (1.05, 0.7). The other interactions with the helicate are weak and include the H··H and the P-F···H-C interactions.

As discussed in chapter 3, compound **1** is a mixed spin dinuclear compound where Fe1 and Fe2 exhibit the HS and LS spin states, respectively. The Hirshfeld surface of the chloride guest ion indicates the difference in Cl···H-N strength of the two iron centers (Figure 6.5 b). The N-H groups near Fe1 exhibit stronger interactions with the chloride guest as indicated by the red color at the surface. This difference in both the Cl···H-N and O···H-N interactions near both iron centers yield this mixed spin state. The same behavior was observed in compound **2**, however, the difference in the Br···H-N interactions at both helical sides are less important. The fingerprint plots of compounds **1** and **2** (Figure 6.5 d and e) are very similar. The only difference is the strength of the X···H-N interactions, which yield similar SCO behavior with only a shift in the $T_{1/2}$ of the transition as seen in chapter 3. The stronger Cl···H-N stabilize the LS state in Fe2 more than the Br···H-N interactions.

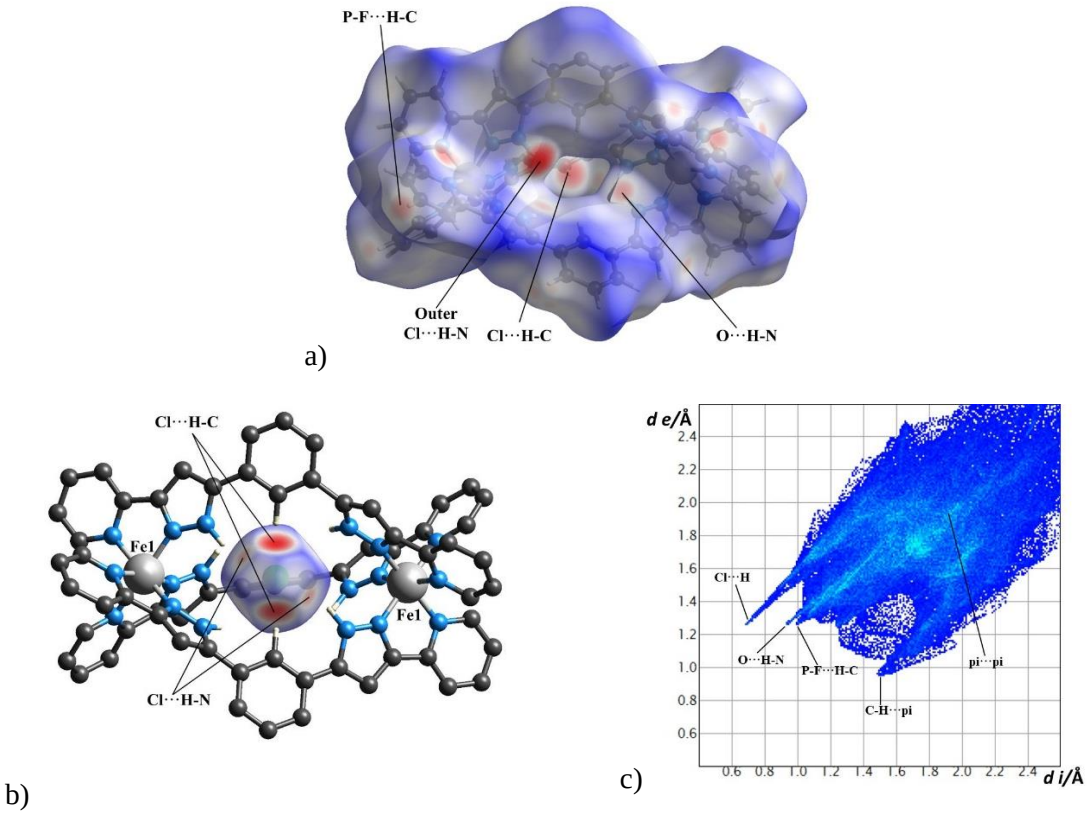

Figure 6.6: Hirshfeld surface of the a) $[Fe_2(H_2L4)_3]^{4+}$ cation from compound **1a**, b) chloride guest in compound **1a**, and c) the 2*D* fingerprint derived from the helicase's Hirshfeld surface.

Compound **1a** is produced by exposing crystals of compound **1** to the ambient water for one week in single-crystal-to-single-crystal transformation. The Hirshfeld surface of the $[Fe_2(H_2L4)_3]^{4+}$ helicate and the chloride guest in compound **1a** and the fingerprint plot of the $[Fe_2(H_2L4)_3]^{4+}$ helicate are seen in Figure 6.6. Now the chloride ion locates in the center of the helicate, as seen by the Hirshfeld surface of this guest, where the interactions are symmetrical. The Cl···H-C contacts are now stronger than the Cl···H-N ones and the latter are symmetrical, near both iron sides. Interestingly, the inner Cl···H-N interactions in compound **1a** are weaker than that in compound **1**. The fingerprint plot of compound **1a** exhibits some differences with respect to **1**. The overall Cl···H interactions are shorter in **1a** thanks to the short Cl···H-C contacts and to the outer Cl···H-N interactions which are now stronger than the O···H-N ones, contrary to what is seen in compound **1**. The C-H···pi interactions in compound **1a** are slightly stronger than these in compound **1**. Moreover, the pi-pi interactions are more intense in **1a**, which indicates closer helicates. It should be noticed that the outer chloride and the methanol molecule are disordered in two positions and the interactions of only one of

these positions are shown in Figure 6.6a. All of these differences yielded a different SCO behavior, where now both iron centers exhibit SCO in two-step fashion. The same differences were observed in compound **2a**, when compared to compound **2**.

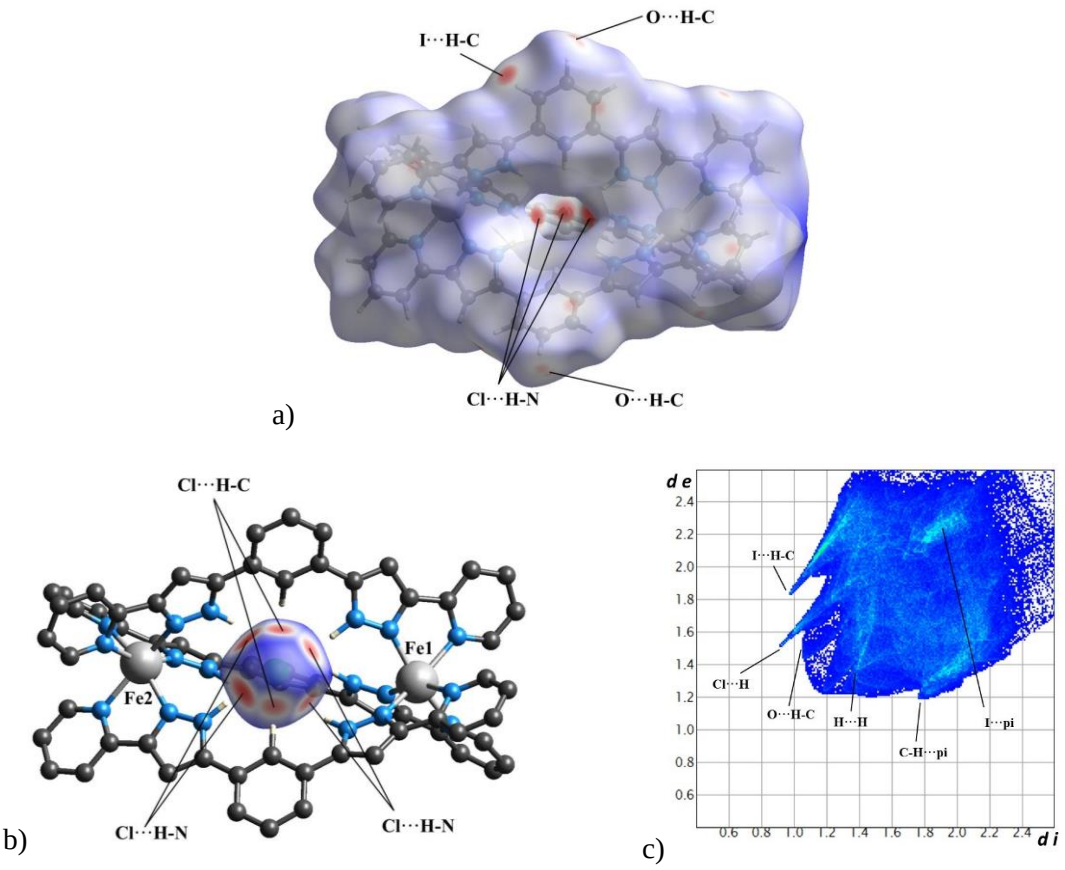

Figure 6.7: Hirshfeld surface of the a) $[Fe_2(H_2L4)_3]^{4+}$ cation from compound **3**, b) chloride guest in compound **3**, and c) the 2*D* fingerprint derived from the Hirshfeld surface of the helicate.

The Hirshfeld surface of the $[Fe_2(H_2L4)_3]^{4+}$ helicate and the chloride guest in compound **3**, and the fingerprint plot of the $[Fe_2(H_2L4)_3]^{4+}$ helicate are seen in Figure 6.7. This complex stays In the HS state overall temperatures. This difference from the previous helicates can be understood from the absence of important interactions with anions or solvent molecules out of the cavity. As seen in Figure 6.7 a, the most important interactions close to the iron centers are those of the inner chloride guest. The interactions with the guest chloride are more symmetrical than these seen in compound **1**. The triodide ions and the ether molecules interact weakly with C-H groups, which are far from the iron centers. The fingerprint plot shows how week these interactions

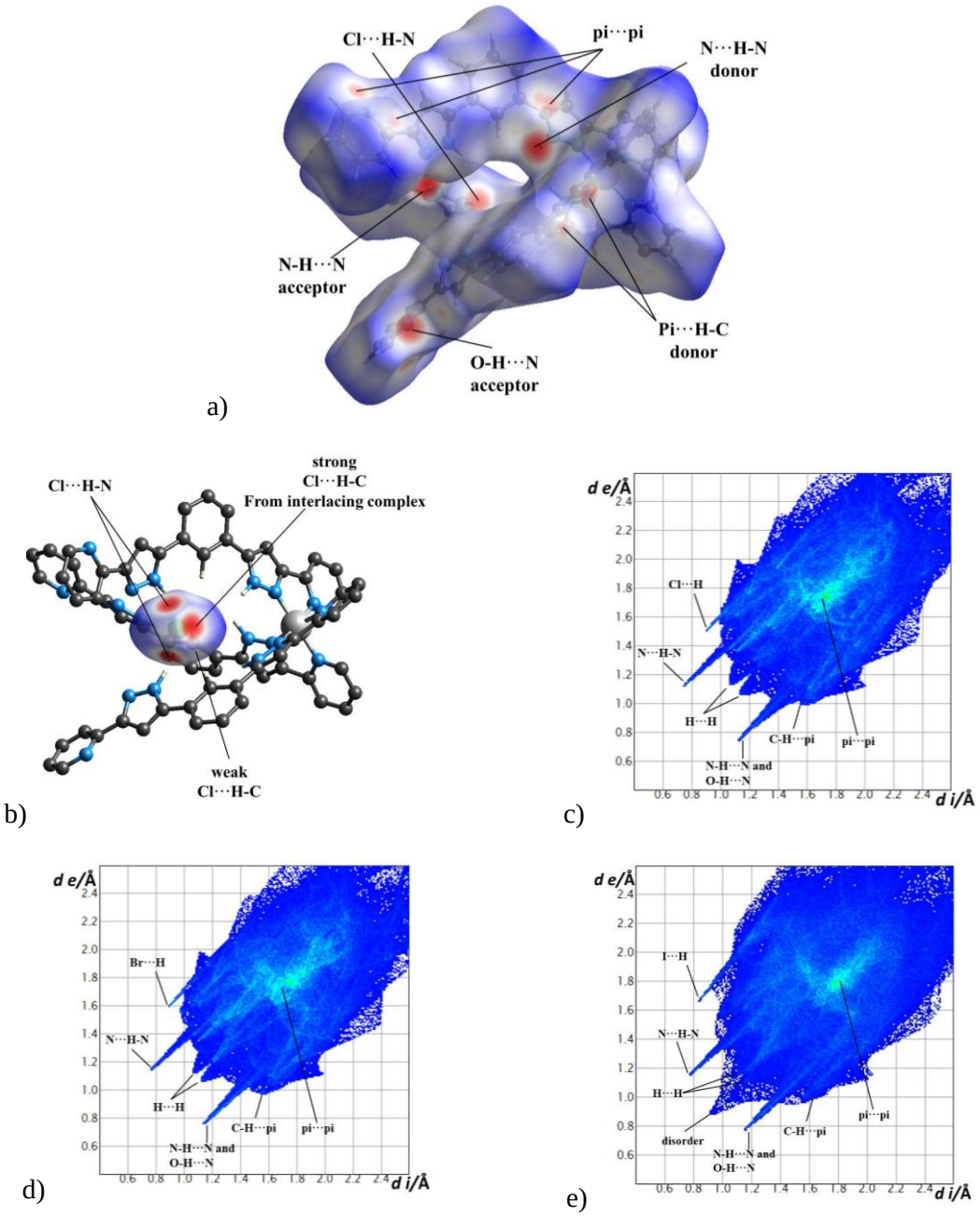

Figure 6.8: Hirshfeld surface of the a) $[Fe(H_2L4)_3]^{2+}$ cation from compound **5**, b) chloride guest in compound **5**, and the 2*D* fingerprint derived from the helicase's Hirshfeld surfaces of compounds **5** (c), compound **7** (d) and compound **9** (e).

comparing to these seen in compounds **1** and **1a**. A similar behavior was observed in compound **4** compared to compounds **2** and **2a**.

For the dimerized mononuclear helicates (chapter 4), three compounds (**5**, **7** and **9**) were chosen as representative for the Hirshfeld surface analysis. The Hirshfeld surface for

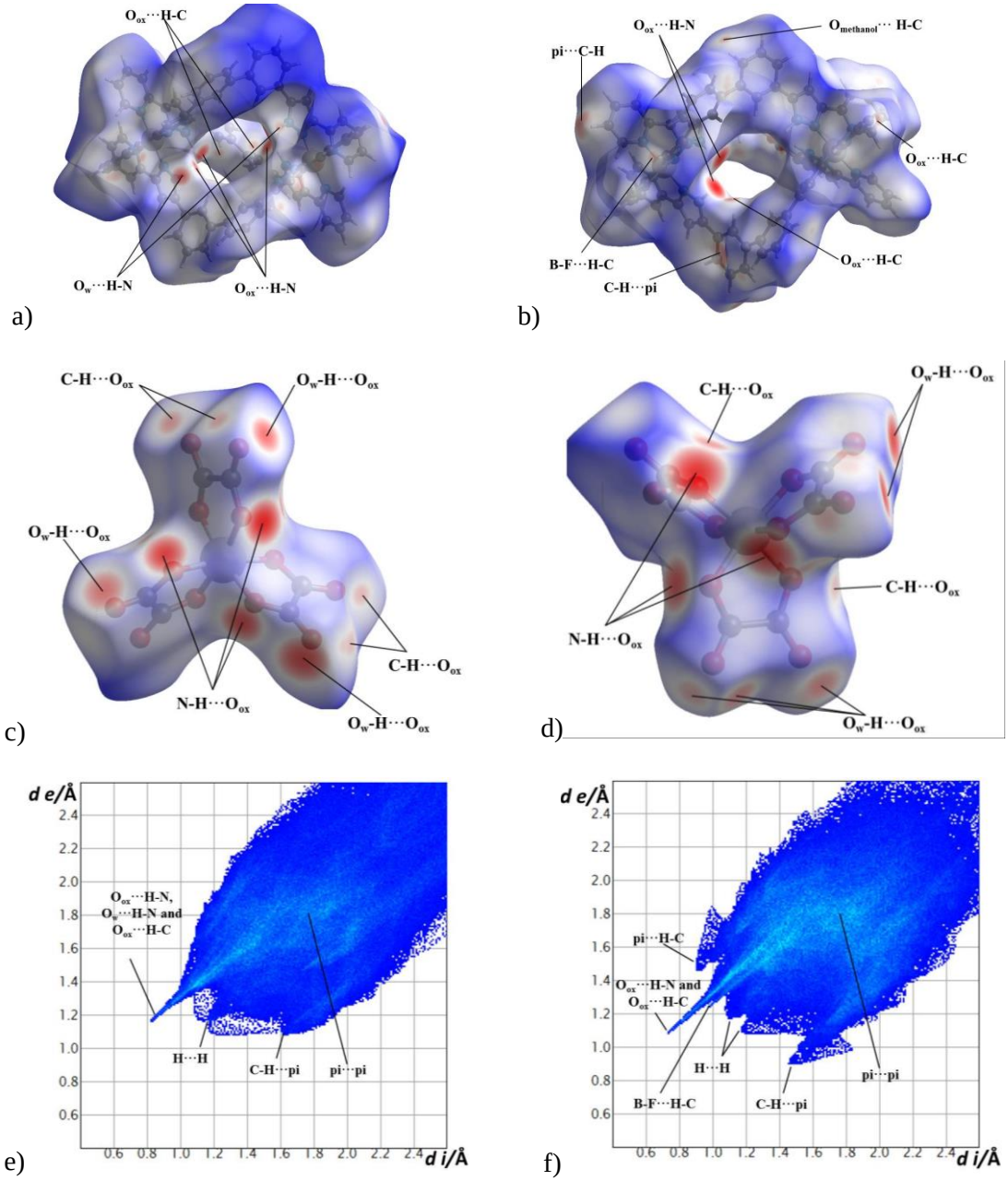

Figure 6.9: Hirshfeld surface of the a) $[Fe_2(H_2L6)_3]^{4+}$ cation from compound **10**, b) $[Fe_2(H_2L6)_3]^{4+}$ cation from compound **11**, c) $[Cr(oxalate)_3]^{3-}$ anion from compound **10**, d) $[Cr(oxalate)_3]^{3-}$ anion from compound **11** and the 2D fingerprint derived from the helicase's Hirshfeld surfaces of compounds **10** (e) and compound **11** (f).

the $[Fe(H_2L4)_3]^{2+}$ complex and the chloride guest in compound **5**, and the fingerprint plots of the $[Fe(H_2L4)_3]^{4+}$ moities in compounds **5**, **7** and **9** are seen in Figure 6.8. Two $[Fe(H_2L4)_3]^{4+}$ units are intertwined together via N-H···N and pi-pi interactions of the pyrazolylpyridine and the benzyl moieties. The interactions with the halide guest help to form this dimerized structure through the N-H···X and the C-H···X interactions.

The terminal non-coordinated pyridine groups are in *trans* configuration and interacting with external OH^- or H_2O species via O-H···N contacts. The chloride guest is interacting symmetrically with both intertwined helicates making them crystallographically identical. The fingerprint plots for the three compounds are very similar where the only important difference is the strength of the X···H interactions, which follow the trend $Cl^->Br^->I^-$. This affects the SCO behavior as discussed in chapter 4. The difference in the H···H region in the fingerprint plot of compound **9** arises from the disorder and the interactions with acetone molecules. However, these interactions are far from the iron centers and do not affect the SCO behavior. It needs to be noted the green color in the region near [1.8,1.8], indicating a high number of pi-pi interactions in these compounds, which occurs between the intertwined complexes.

The Hirshfeld surface of the $[Fe_2(H_2L6)_3]^{4+}$ helicate and the oxalate guest in compound **10** and **11** and the fingerprint plots of the $[Fe_2(H_2L4)_3]^{4+}$ helicate in the same compounds are seen in Figure 6.9. The main interactions between the oxalate and the helicate are these between the pyrazole groups and the coordinated oxalate oxygen. The non-coordinated oxygen atoms of the oxalate are interacting with water molecules or C-H groups from other helicates. For compound **10**, some water molecules are close to the helicates and form interactions with the pyrazole groups too. These water molecules are important to form the solid state network of the host-guest system as discussed in chapter 5. The most important interactions within the host-guest system are these inside the cavity as seen in Figure 6.9. The interactions between the oxalate guest and the helicate are stronger in compound **11** than in compound **10**. Moreover, the helicates of compound **11** interact more strongly than in compound **10**, mainly with C-H···pi and pi-pi interactions. Although these two compounds are isostructural, the small differences in the intermolecular interactions yielded different SCO behavior.

6.4 **Conclusions**

Using the x-ray structural data available for the pyrazolylpyridine based complexes in this thesis and similar one in the literature, the correlation between the local distortions around the metal ion and the spin state of the latter was studied. The distortion parameters Σ and Θ were used to correlate the spin state of the Fe(II) centers in these complexes. Each spin state displays a clear range and these parameters can be used to distinguish between systems fully in one state or the other. The continuous symmetry

measures were also used to study the local distortion of the Fe(II) centers. As expected, the HS cations are distorted more than the LS cations from the octahedral geometry toward trigonal prism. A determining factor for the spin state of the Fe(II) centers is the nature and the strength of the different supramolecular intermolecular interaction around these metal ions. To study and visualize the supramolecular interactions of the helicates with guests or anions or solvent molecules, Hirschfield surfaces analysis was used. Here, the small differences in the supramolecular interactions can be seen using the 2*D* finger prints.

6.5 References

1 M. A. Halcrow, *Coord. Chem. Rev.*, 2009, **253**, 2493–2514.

2 M. A. Halcrow, *Chem. Soc. Rev.*, 2011, **40**, 4119–4142.

3 G. A. Craig, J. S. Costa, O. Roubeau, S. J. Teat and G. Aromí, *Chem. - A Eur. J.*, 2012, **18**, 11703–11715.

4 L. A. Barrios, E. Peyrecave-Lleixá, G. A. Craig, O. Roubeau, S. J. Teat and G. Aromí, *Eur. J. Inorg. Chem.*, 2014, **2014**, 6013–6021.

5 P. Guionneau, M. Marchivie, G. Bravic, J.-F. Létard and D. Chasseau, *Top. Curr. Chem.*, 2004, **234**, 97–128.

6 S. Alvarez, *J. Am. Chem. Soc.*, 2003, **125**, 6795–6802.

7 J. M. Holland, J. A. McAllister, C. A. Kilner, M. Thornton-Pett, A. J. Bridgeman and M. A. Halcrow, *J. Chem. Soc. Trans.*, 2002, **2**, 548–554.

8 J. J. McKinnon, A. S. Mitchell and M. A. Spackman, *Chem. - A Eur. J.*, 1998, **4**, 2136–2141.

9 A. Grosjean, N. Daro, B. Kauffmann, A. Kaiba, J.-F. Létard and P. Guionneau, *Chem. Commun. (Camb).*, 2011, **47**, 12382–4.

10 H. J. Shepherd, P. Rosa, L. Vendier, N. Casati, J.-F. Létard, A. Bousseksou, P. Guionneau and G. Molnár, *Phys. Chem. Chem. Phys.*, 2012, **14**, 5265.

11 G. A. Craig, J. S. Costa, O. Roubeau, S. J. Teat and G. Aromí, *Eur. J. Inorg. Chem.*, 2013, 745–752.

12 P. Wei, D. Yuan, W. Zhu, X. Zhang and B. Hu, *Acta Crystallogr. Sect. E Struct. Reports Online*, 2010, **66**, m190–m191.

13 L. F. Jones, C. A. Kilner and M. A. Halcrow, *J. Clust. Sci.*, 2010, **21**, 279–290.

14 L. S. Harimanow, K. H. Sugiyarto, D. C. Craig, M. L. Scudder and H. A. Goodwin, *Aust. J. Chem.*, 1999, **52**, 109–122.

15 K. Yoneda, K. Adachi, K. Nishio, M. Yamasaki, A. Fuyuhiro, M. Katada, S. Kaizaki and S. Kawata, *Angew. Chemie - Int. Ed.*, 2006, **45**, 5459–5461.

16 T. Shiga, M. Noguchi, H. Sato, T. Matsumoto, G. N. Newton and H. Oshio, *Dalton Trans.*, 2013, **42**, 16185–93.

17 L. Hao, T. Liu, J. Chen and X. Zhang, *Acta Crystallogr. Sect. E Struct. Reports Online*, 2010, **66**.

18 T. Shiga, E. Oshiro, N. Nakayama, K. Mitsumoto, G. N. Newton, H. Nishikawa and H. Oshio, *Eur. J. Inorg. Chem.*, 2013, 781–787.

19 S. Vela, J. J. Novoa and J. Ribas-Arino, *Phys. Chem. Chem. Phys.*, 2014, **16**, 27012–24.

20 S. Alvarez, D. Avnir, M. Llunell and M. Pinsky, *New J. Chem.*, 2002, **26**, 996–1009.

21 S. K. Wolff, D. J. Grimwood, J. J. McKinnon, M. J. Turner, D. Jayatilaka and M. A. Spackman, 2012, University of Western Australia.

22 M. A. Spackman and J. J. Mckinnon, 2002, **4**, 378–392.